Could the two anticyclonic eddies during winter 2003/2004 be reproduced and predicted in the northern south China sea?

Dazhi Xu [1,3], Wei Zhuang[4], Youfang Yan [2*]

[1]South China Sea Marine Prediction Center, State Oceanic Administration, Guangzhou, China

[2]South China Sea Institute of Oceanology, Chinese Academic of Science, Guangzhou, China

[3]Nansen Environmental and Remote Sensing Center, Bergen, Norway

[4] State Key Laboratory of Marine Environmental Science & College of Ocean and Earth Sciences, Xiamen University, Xiamen 361102, China

Abstract

Great progress has been made in understanding the mesoscale eddies and their role on the large-scale structure and circulation of the oceans. However, many questions still remain to be resolved, especially with regard to the reproductivity and predictability of mesoscale eddies. In this study, the reproductivity and predictability of mesoscale eddies in the Northern SCS (NSCS), a region with strong eddy activity, are investigated with a focus on two typical anticyclonic eddies (AE1 and AE2) based on a HYCOM-EnOI Assimilated System. The comparisons of assimilated results and observations suggest that generation, evolution and propagation paths of AE1 and AE2 can be well reproduced and forecasted when the observed amplitude >8 cm (or the Advective nonlinearity parameter $U/c > 2$), although their forcing mechanisms are quite different. However, when their amplitudes are less than 8 cm, the generation and decay of these two mesoscale eddies cannot be well reproduced and predicted by the system. This result suggests, in addition to dynamical mechanisms, the spatial resolution of assimilation observation data and numerical models must be taken into account in reproducing and predicting mesoscale eddies in the NSCS.

Keywords: HYCOM; EnOI; Northern South China Sea; Mesoscale eddy; Predictability

1. Introduction

Equivalent to the synoptic variability of the atmosphere, the ocean mesoscale eddies is often described as the "weather" of the ocean, with typical spatial scales of ~100 km and time scales of a month (Chelton et al., 2011; Liu et al., 2001; Wang et al., 1996). The mesoscale eddy is characterized by temperature and salinity anomalies with associated flow anomalies, exhibiting different properties to their surroundings, thus allowing them to control the strength of mean currents and to transport heat, salt, and biogeochemical tracers around the ocean. Although today, the beauty and complexity of these mesoscale features can be seen by viewing high resolution satellite images or numerical model simulations (Yang et al., 2000; Fu et al., 2010; Morrow and Le Traon, 2012; Frenger et al., 2013), the operational forecasts of the mesoscale eddy still pose a big challenge because of its complicated dynamical mechanisms and high nonlinearity (Woodham, et al. 2015; Treguier, et al. 2017; Vos et al. 2018). A recent example is the explosion of the Deepwater Horizon drilling platform in the northern Gulf of Mexico in 2010 where an accurate prediction of the position and propagation of the Loop Current eddy was essential in determining if the spilled oil would be advected to the Atlantic Ocean or still remain within the Gulf (Treguier et al., 2017).

Similar to Gulf of Mexico, the South China Sea (SCS) is also a large semi-closed marginal sea in the northwest Pacific, connecting to the western Pacific through the Luzon Strait (Fig. 1). Forced by seasonal monsoon winds, the intrusion of Kuroshio Current (KC), the Rossby waves and the complex topography, the SCS, especially the Northern SCS (NSCS) exhibits a significantly high mesoscale eddy activity (Fig. 2).

Many studies have tried to investigate the mesoscale eddy in the NSCS (Wang et al., 2003; Jia et al., 2005; Wang et al., 2008). Based on the potential vorticity conservation equation and in-situ survey data, Yuan and Wang (1986) pointed out that the bottom topography forcing might be the primary factor for the formation of anticyclonic eddies in the northeast of Dongsha Islands (DIs). Using survey CTD data in September 1994, Li et al. (1998) recorded the evidence of anticyclonic eddies in the NSCS and suggested these anticyclonic eddies are probably shed from the KC. Investigations by Wu et al. (2007) showed that westward propagating eddies in the NSCS originate near the Luzon Strait rather than coming from the western Pacific. Based on the altimeter, the trajectory of drift and hydrological observations data, Wang et al. (2008) studied the evolution and migration of two anticyclonic eddies in the NSCS during winter of 2003/2004. As they described, the AE1 generated by interaction of the unstable rotating fluid with the sharp topography of DIs firstly appeared near DIs on the 10th of December 2003 (see Fig. 3). Then it began to move southwestward with its amplitude decreasing gradually. During the movement of AE1, another anticyclonic eddy (AE2) was shed and developed from the loop current of Kuroshio near the Luzon Strait on the 14th of January 2004. The amplitude of AE2 was then increased when it propagated southwestward (Fig. 3d-3f). About five weeks later, AE2 reached its maximum in amplitude and then lasted around three weeks in its mature state. During its decay phase, AE2 moved southwestward quickly with its amplitude decreasing, and finally disappeared at the location of 114°E, 18°N on the 7th of April 2004. In the meanwhile, AE1 continued moving to southwest and eventually disappeared in the southeastern of Hainan. These

64 studies improved our understanding of activities of mesoscale eddy and its possible
65 dynamical mechanisms in the NSCS.

66 Despite the studies on the activities and its possible dynamical mechanisms of
67 mesoscale eddies in the NSCS have received much attention in past decades, studies on
68 the reproductivity and predictability of mesoscale eddies in the NSCS are still rare. As
69 mentioned above, mesoscale eddies are not only related to complicated dynamical
70 mechanisms but also involve strong nonlinear processes (Oey et al., 2005) thus they are
71 not a deterministic response to atmospheric forcing. The quality of mesoscale eddies
72 forecasting will depend primarily on the quality of the initial conditions. Ocean data
73 assimilation, which combines observations with the numerical model, can provide more
74 realistic initial conditions and thus is essential for the prediction of mesoscale eddies
75 (Xiao et al. 2006; Xie et al. 2011; Xu et al. 2012; Xie et al. 2018). In this study, we
76 assessed the reproduction and predictability of two typical anticyclonic eddies in the
77 NSCS with focus on their generation, evolution and decay processes by a series of
78 numerical experiments based on a Chinese Shelf/Coastal Seas Assimilation System
79 (CSCASS; Li, 2009; Li et al., 2010; Zhu, 2011) along with the observation data from
80 surface drifter trajectory and satellite remote sensing.

81 **2. Datasets and Methodologies**

82 **2.1 Datasets**

83 In this study, the altimetric data between 2003-2004, which includes along-track
84 SLA, totally 29 passes (about 9300 points) over the domain of CSCS was selected.

Considering the noise of SLA measurement in the shallow seas, data for the shallow areas with depth<400 m was excluded. In order to verify, the merged SLA based on Jason-1, TOPEX/Poseidon, ERS-2 and ENVISAT (Ducet et al., 2000) provided by Archiving, Validation and Interpretation of Satellites Oceanographic data (AVISO) at Centre Localization Satellite (CLS, ftp://ftp.aviso.oceanobs.com/global/nrt/) with 1/4° x 1/4° resolution and weekly average are used. In addition, because the SLA present only the anomalies relative to a time-mean sea level field, thus a new mean dynamic topography (nMDT), which has been corrected using iterative method by Xu et al. (2012) was used to calculate the realistic sea level in this study.

In addition to SLA datasets, the daily OISST from the National Oceanic and Atmospheric Administration's (NOAA) National Climatic Data Center (ftp://eclipse.ncdc.noaa.gov/pub/OI-daily-v2/NetCDF/), which was merged by an optimum interpolation method (Reynolds et al., 2007) based on the Infrared SST collected by the Advanced Very High Resolution Radiometer sensors on the NOAA Polar Orbiting Environmental Satellite and SST from Advanced Microwave Scanning Radiometer for the Earth Observing System are also used. The daily OISST's biases were fixed using in situ data from ships and buoys. The dataset between 2003 and 2004 was used in this study, with a spatial resolution of 1/4°×1/4°. In addition, the surface drifting buoy data from the World Ocean Circulation Experiment (WOCE, ftp://ftp.aoml.noaa.gov/pub/phod/buoydata/) are also used. A total of 3 drifters designed to drift at the surface within the upper 15 m and tracked by the ARGOS satellite system. Positions of the drifters were smoothed using a Gaussian-filter scale of 24 h to eliminate

tidal and inertial currents, and were subsampled at 6-h intervals (Hamilton et al., 1999).

2.2 Method of identify the mesoscale eddies

Similar to the standard of Chelton et al., (2011) and Cheng et al., (2005), we identify the mesoscale eddies in this study is as follows: 1) there must be a closure contour on the merged SLA; 2) there must have one maximum or minimum inside the area of closure contour for anticyclonic or cyclonic eddy; 3) the difference between the extremum and the outermost closure of SLA, that is, the amplitude of the mesoscale eddy must be greater than 2 cm; and 4) the spatial scale of the eddy should be 45-500 km. In addition, the amplitude (A) of an eddy is defined here to be the magnitude of the difference between the estimated basal height of the eddy boundary and the extremum value of SSH within the eddy interior: $A=|h_{ext}-h_0|$.

2.3 Ocean model

We here used a three-dimensional hybrid coordinate ocean model (HYCOM; Bleck, 2002; Halliwell et al., 1998; 2000; Halliwell, 2004; Chassignet et al., 2007) to provide a dynamical interpolator of observation data in the assimilation system. HYCOM is a primitive equation general ocean circulation model with vertical coordinates: isopycnic coordinate in the open stratified ocean, the geopotential (or z) coordinate in the weak stratified upper ocean, and the terrain following sigma-coordinate in shallow coastal regions.

In this study, HYCOM was implemented in the Chinese shelf/coastal seas with a horizontal resolution of 1/12°×1/12°, and in the remaining regions with 1/8°×1/8°, the model domain is from 0°N to 53°N and from 99°E to 143°E, the detail model domain

129 and grid can refer to the inset panel of Fig.1. The vertical water column from the sea
130 surface to the bottom was divided into 22 levels. The K-Profile Parameterization (KPP;
131 Large et al., 1994), which has proved to be an efficient mixing parameterization in many
132 oceanic circulation models, was used here. The bathymetry data of the model domain
133 were taken from the 2-Minute Gridded Global Relief Data (ETOPO2).

134 To adjust the model dynamics and achieve a perpetually repeating seasonal cycle
135 before applying the interannual atmospheric forcing, the model was initialized with
136 climatological temperature and salinity from the World Ocean Atlas 2001 (WOA01;
137 Boyer et al., 2005) and was driven by the Comprehensive Ocean-Atmosphere Data Set
138 (COADS; Woodruff et al., 1987) in the spin-up stage. After integrating ten model years
139 with climatological forcing, the model was forced by the European Center for Medium-
140 Range Weather Forecasts (ECMWF) 6-hourly reanalysis dataset (Uppala et al., 2005)
141 from 1997 to 2003. The wind velocity (10-m) components were converted to stresses
142 using a stability dependent drag coefficient from Kara et al. (2002). Thermal forcing
143 included air temperature, relative humidity and radiation (shortwave and longwave)
144 fluxes. Precipitation was also used as a surface forcing from Legates et al. (1990).
145 Surface latent and sensible heat fluxes were calculated using bulk formulae (Han, 1984).
146 Monthly river runoff was parameterized as a surface precipitation flux in the ECS, the
147 SCS and Luzon Strait (LS) from the river discharge stations of the Global Runoff Data
148 Centre (GRDC) (http://www.bafg.de), and scaled as in Dai et al. (2002). Temperature,
149 salinity and currents at the open boundaries were provided by an India-Pacific domain
150 HYCOM simulation at 1/4° spatial resolution (Yan et al., 2007). Surface temperature

and salinity were relaxed to climate on a time scale of 100 days. Both two-dimensional barotropic fields such as Sea Surface Height and barotropic velocities, and three-dimensional baroclinic fields such as currents, temperature, salinity and density were stored daily.

2.4 The assimilation scheme

The ensemble optimal interpolation scheme (EnOI; Oke et al., 2002), which is regarded as a simplified implementation of the Ensemble Kalman Filter (EnKF), aims at alleviating the computational burden of the EnKF by using stationary ensembles to propagate the observed information to the model space. The data assimilation schemes can be briefly written as (Oke et al., 2010):

$$\vec{\psi}^{a} = \vec{\psi}^{b} + K(\vec{d} - H\vec{\psi}^{b}) \tag{4}$$

$$K = P^{b}H^{T}[HP^{b}H^{T} + R]^{-1} \tag{5}$$

where $\vec{\psi}$ is the model state vectors including model temperature, layer thickness and velocity; Superscripts a and b denote analysis and background, respectively; $\vec{d}$ is the measurement vector that consists of SST and SLA observations; K is the gain matrix; and H is the measurement operator that transforms the model state to observation space. P is the background error covariance and R is the measurement error covariance. In EnOI, Eq. 5 can be expressed as:

$$K = \alpha(\sigma \circ P^{b})H^{T}[\alpha H(\sigma \circ P^{b})H^{T} + R]^{-1} \tag{6}$$

where α is a scalar that can tune the magnitude of the analysis increment; σ is a correlation function for localization; and P^{b} is the background error covariance which

can be estimated by

$$P^b = A' A'^T /(n-1) \quad (7)$$

In Eq. 7, n is the ensemble size, A' is the anomaly of the ensemble matrix, $A=(\psi_1,\psi_2,\cdots,\psi_N)\in\Re^{n\times N}$ ($\psi_i\in\Re^N(i=1,\cdots,n)$ is the ensemble members, N is the dimension of the model state, representing usually the model variability at certain scales by using a long-term model run or spin-up run. More detailed description and evaluation of the CSCASS in Li et a., (2010) and Xu et al., (2012).

3. Results

3.1 The reproduction of these anticyclonic eddies in the NSCS

In order to investigate whether the evolution and migration features of these two eddies can be reproduced by the CSCASS or not, we firstly set up an assimilation experiment named As_exp (see Fig. 4, black line) for AE1 and AE2. In this experiment, the observed SST and SLA are both assimilated into CSCASS at an equal interval of every 3 days. To meet dynamic adjustment, the first assimilation was performed on the 27th of September 2003, two months prior to the generation of AE1.

Base on the As_exp experiment output, we use the observations SLA to evaluate the uncertainty of CSCASS in the eddies area. In this study, we calculated the weekly mean RMS error (RMSE) of the As_exp /control experiments output and observations for SLA. As the result indicates, the RMSE for the As_exp is between 6 cm to 14 cm, while RMSE for the control is between 10 cm to 18 cm. This result suggested that data assimilation improved effectively the SLA field and had a beneficial impact on model

194 results in this area.

195 In addition, we also use the advective nonlinearity parameter (Chelton et al., 2011;
196 Li et al., 2014; 2015; 2016; Wang et al., 2015) as a criterion to estimate the eddy forecast
197 ability of the CSCASS. As fig. 5 shows, when the advective nonlinearity parameter
198 greater than 2 (that is the amplitude greater than 8 cm) AE2 can be well reproduced by
199 the CSCASS.

200 Besides, we also use the independent evaluation, figure 6 compared the
201 assimilating results of AE1 with the observations both from the satellite remote sensing
202 and drifter buoys trajectories of number 22517, 22918 and 22610 between December
203 3rd 2003 and February 18th 2004. From Fig. 6 and Table 1, we can see that the generation
204 and movement of AE1 can be well reproduced by the CSCASS, with the pink curves
205 (assimilation) match well with those of black (satellite observations) and dotted lines
206 (the trajectories of drifter buoys). In addition, the spatial pattern of AE1 can also be well
207 revealed by the CSCASS: the radius of meridional and zonal of AE1 detected by the
208 assimilation are 163 km and 93 km, which are almost equal to that of observations (148
209 km and 79 km). The migration path of AE1 can also be well reproduced by the CSCASS
210 (see Fig. 6, black and pink line) until its amplitude decays to less than 8 cm. In addition
211 to AE1, the generation and evolution of AE2 are also evaluated. As shown Fig. 7, the
212 evolution and propagation pathway of AE2 (Fig. 7b-7j), e.g., move northwestward
213 firstly and then southwestward can generally be reproduced by the CSCASS, although
214 its initial location shows a slight southward bias in the simulation (Fig. 7a). Similar to
215 the results of AE1, discrepancies between model and observations become larger again

during the decay phase of AE2.

In general, the comparison of assimilation SLA with that of satellite observation and the trajectories of drifter buoys suggested that the generation, development and the propagation of AE1 and AE2 can be reproduced by the CSCASS when their amplitude greater than 8 cm. However, when their intensity are relatively weak, with amplitudes less than 8 cm, the features of these two mesoscale eddies are not well reproduced by the CSCASS. This may be related to the value setting of parameter α, the localization length scale, and insufficient spatial resolution of assimilating SSH or the numerical model (Counillon and Bertino, 2009).

3.2 The predictability of these anticyclonic eddies in the NSCS

Since the generation, development and the propagation of AE1 and AE2 can be well reproduced by the CSCASS when their amplitude >8 cm, as mentioned above, in this section we further use the CSCASS to investigate the predictability of these two eddies. According to the generation, evolution and migration of these two eddies, we designed six forecast experiments, hereafter referred to as Exp1 to Exp6 (see Fig. 4) to investigate their predictability. The model's initial state prior to each of the six forecast experiments is constrained by assimilating satellite SLA and SST before. Based on the initial state, each experiment is run forward 30 days with the forcing of 6-hourly wind, surface heat flux, and monthly mean river runoff, etc. The first experiment, named Exp1, is applied on the 29th of November 2003, which tends to study whether the generation of AE1 can be forecasted or not. Exp2 is implemented on the 10th of December 2003 and is used to study whether the development and the migration of AE1 can be

forecasted. Exp3 is run based on the initial state on the 31th of December 2003 and used to show whether the generation of AE2 and the continued migration of AE1 can be forecasted. In order to investigate whether the continued evolution of AE1 and AE2 can be forecasted, Exp4 is applied on the 21th of January 2003. Exp5, is setting up to reveal whether the attenuation of AE1 and the evolution of AE2 can be forecasted, while Exp6 which is applied on the 29th of February 2004 was designed to find out whether the disappear of AE1 and AE2 can be forecasted.

The prediction results of Exp1 are shown in Fig. 8. In Fig. 8a, we can see that the forecast is almost coincident with the satellite observation and the trajectory of drift buoys, indicating that the generated position of AE1 can be well forecasted by the CSCASS. In addition, the initial migration of AE1 can also be forecasted by the CSCASS (see Fig. 8a and 8f). In order to evaluate the forecasted amplitude of AE1, the intensity, amplitude and the distance of eddy centers between the observation and the forecast are also quantified (Table 2: EXP1). From Table 2: EXP1, we can see that the amplitude of forecasting matches well with that of observation, although its amplitude is slightly larger than that of observation. After 4 weeks, the amplitude and intensity of the forecast are still close to those of the observation, suggesting that the generation of AE1 can be well predicted by the CSCASS.

In order to find out whether the development and movement path of AE1 can be predicted after generation, we continue to carry out Exp2. As shown by the observation (Fig. 9), AE1 moves southwestward along the continental shelf with its amplitude decreasing and again increasing after its generation. This observed southwestward

movement is also predicted by the CSCASS (see pink closure curve in Fig. 9a-9d), although a sudden southwestward movement cannot be well predicted (Fig. 9f). In addition, the first attenuation and then enhance of AE1 can also been predicted by the CSCASS (see Table 2 and Fig. 9b). On the whole, the development and movement path of AE1 can be well predicted by CSCASS for the first four weeks after its generation. After that, the errors between observation and prediction increase significantly, and by the fifth week, the distance between the center of the prediction and the observation become larger, which more than 100 km (see Fig. 9e).

For further analysis, we carry out Exp3, to look at whether the continue evolution of AE1 and the generation of AE2 can be predicted. This experiment is carried out based on the initial condition of the assimilation on the 31st of December 2003 and the corresponding results are shown in Fig. 10 and Table 2. The development trend of AE1 can be predicted, but with a slightly weak amplitude, as shown by the prediction (Fig. 10, Table 2). The observed center elevation of AE1 reduced from 18 cm in the first week to 13 cm in the fifth week. Similar decreasing trend was also found for the forecast but with its amplitude decreasing from 13 cm at the beginning to 10 cm at the end of the forecast period. Although the decreasing trend of AE1 amplitude is quite similar between the observations and forecast, their intensity is slightly different. In addition, the movement path of AE1 cannot be accurately predicted at this period, for instance, the observed AE1 moves directly to southwest (see red solid line and solid circle in Fig. 8f), but the prediction's movement firstly toward northeast, then turns to southwest (see blue solid line and solid circle in Fig. 10f). The generation of AE2 cannot be predicted

282 in Exp3, which may be related to the lower amplitude (<8 cm) of AE2 at this period.

283 The purpose of Exp4 is to look at whether the evolution of AE1 and AE2 can both
284 be reasonably predicted. Since this experiment mainly focuses on the evolution of AE1
285 and AE2, thus Fig. 11 shows only the evolution of AE2 from the second week after
286 generation, that is, from the beginning on the 21st of January 2004 to the fifth week. As
287 shown in Fig. 11, Table 2 and Fig. 14d, the trends of amplitude variation of both eddies
288 can be well predicted with the decreasing of AE1 and slowly increasing of AE2. For
289 AE1, the results of the prediction and observation are very close in the first two weeks,
290 with the center of the two almost coincide. The central position of the prediction and
291 observation began to deviate after the third week. For AE2, although the amplitude and
292 movement path are not predicted well at its initial stage, the prediction is slowly
293 approaching to the observation during third to fifth week, and distance between the
294 center of the prediction and the observation is reduced from 132 km at the beginning to
295 81 km at the end (see Fig. 14d the black line).

296 As mentioned above, the purpose of Exp5 is to investigate whether the decay of
297 AE1 and the continued development of AE2 can be predicted. From Fig. 12, Table 2
298 and Fig. 14e, we can find that the CSCASS cannot predict the movement path of AE1
299 well in its decay stage: the distance between the center of the prediction and that of the
300 observation is greater than 188 km, and the moving direction of the two is not consistent
301 (see red lines and dots in Fig. 12f). But the evolution and moving direction of AE2 can
302 be well predicted at this stage. The amplitude of observation and prediction of AE2 are
303 keeping in the consistent trend (Fig. 14e), although the speed of movement of AE2

given by prediction is slower than that of observation (see green lines and dots in Fig. 12f).

The aim of Exp6 is to find whether the disappearance of AE1 and AE2 can be both predicted. As described in Fig. 13, the disappearance of AE1 cannot be well predicted since the low amplitude (less than 8 cm) of AE1 at this stage. Similarly, the disappearance of AE2 is also less accurately predicted by the CSCASS (Fig. 14f). The amplitude of AE2 from the observation decays continually at this stage, but the amplitude of the predicted almost keeps constant. In addition, there is large deviation of the direction of movement between prediction and observation for AE2 (see the red solid line and dot in Fig. 13f).

4. Conclusions and challenges for forecasting of mesoscale eddy

In this paper, we carry out a series of assimilation and prediction experiments by the CSCASS to assess the productivity and predictability of mesoscale eddies in the NSCS, along with observations of satellite observed SST, SLA and the trajectory data of drift. The comparisons of AE1 and AE2 by the CSCASS, which is assimilated SLA and SST, with that of observations through predicted experiments shows that when the amplitudes of mesoscale eddy are higher than 8 cm, the generation, development, decay and movement of eddies can be well reproduced, but when the amplitude of the mesoscale eddy is lower than 8 cm, the generation and disappear of mesoscale eddy cannot be well reproduced.

The comparisons of AE1 and AE2 through six predicted experiments with those

of observations also show that the generation, evolution and movement path of these two eddies with high amplitude (>8 cm or U/c > 2) can be well predicted by the CSCASS, although the generative mechanism of these two eddies is quite different [9]. However, when the amplitude of eddies becomes less than 8 cm, the generation position and the movement path cannot be well predicted by the CSCASS.

Our results suggested that for intensity mesoscale eddies, a good initial condition after assimilating observations can help to improve their reproduced and predictable ability. As mentioned above, the mesoscale eddies are related to strong nonlinear processes and are not a deterministic response to atmospheric forcing, thus the quality of mesoscale eddies forecast will depend primarily on the quality of the initial conditions. In addition, the ability of the ocean numerical model to faithfully represent the ocean physics and dynamics is also crucial. Although data assimilation, which combines observations with the numerical model, can provide good initial conditions, it cannot make up the limitations of numerical model in numerical algorithms and in its resolution. For a high-resolution operational oceanography, the latter means that the numerical models need to be improved using more accurate numerical algorithms and resolution especially in the weakly stratified regions or on the continental shelf.

Furthermore, so far most of the information about the ocean variability is obtained remotely from satellites (SSH and SST), the information about the subsurface variability are very rare. Although a substantial source of subsurface data is provided by the vertical profiles (i.e., expendable bathy thermographs, conductivity temperature depth, and Argo floats), the datasets are still not sufficient to determine the state of the

ocean. In addition, in order to accurately assimilate the SSH anomalies from satellite altimeter data into the numerical model, it is necessary to know the oceanic mean SSH over the time period of the altimeter observations (Xu et al., 2011; Rio et al., 2014). This is also a big challenge because the earth's geoid is not presented with sufficient spatial resolution when assimilating SSH in an eddy-resolving model. With the advent of the SWOT (Surface Water and Ocean Topography) satellite mission in 2020, it should be possible to better resolve and forecast the mesoscale features in eddy resolving ocean forecasting systems.

Acknowledgements:

This study is supported by the Marine Science and Technology Foundation of South China Sea Branch, State Oceanic Administration (grant 1447), the National Key Research and Development Program of China (2016YFC1401407), the Project of Global Change and Air-Sea interaction under contract No. GASI-03-IPOVAI-04, the National Natural Science Foundation of China (Grant No. 41776037 and 41276027), and the China Scholarship Council (award to Xu Dazhi for 1 year's study abroad at Nansen Environmental and Remote Sensing Center).

365

366 **References:**

367 Bleck R, 2002. An oceanic general circulation model framed in hybrid isopycnic cartesian
368 coordinates. Ocean Modelling, 4(1): 55-88.

369 Boyer T P, Levitus S, Antonov J I, Locarnini R A, Garcia H E, 2005. Linear trends in salinity
370 for the World Ocean, 1955-1998. Geophysical Research Letters, 32(1): 67-106.

371 Chassignet E P, Hurlburt H E, Smedstad O M, et al., 2007. The HYCOM (Hybrid Coordinate
372 Ocean Model) data assimilative system. Journal of Marine Systems, 65(1-4):60-83.

373 Chelton D B, Schlax M G, Samelson R M, 2011. Global observations of nonlinear mesoscale
374 eddies. Progress in Oceanography, 91(2): 167-216.

375 Cheng X H, Qi Y Q, Wang W Q, 2005. Seasonal and Interannual Variabilities of Mesoscale
376 Eddies in South China Sea. Journal of Tropical Oceanography, 24(4): 51-59.

377 Counillon F, Bertino L, 2009. Ensemble Optimal Interpolation: multivariate properties in the
378 Gulf of Mexico. Tellus, 61A: 296-308.

379 Dai A, Trenberth K E, 2002. Estimates of freshwater discharge from continents: latitudinal and
380 seasonal variations. Journal of Hydrometeorology, 3(6): 660-685.

381 Ducet N, LeTraon P Y, Reverdin G, 2000. Global high-resolution mapping of ocean circulation
382 from TOPEX/Poseidon and ERS-1 and-2. Journal Geophysical Research, 105(C8):
383 19477-19498.

384 Frenger I, Gruber N, Knutti R, Münnich M, 2013. Imprint of Southern Ocean eddies on winds,
385 clouds and rainfall. Nature Geoscience, 6, 608-612.

386 Fu L-L, Chelton D B, Traon P-Y L, Morrow R, 2010. Eddy dynamics from satellite altimetry.
387 Oceanography, 23(4):14-25.

388 Halliwell J G R, 2004. Evaluation of vertical coordinate and vertical mixing algorithms in the
389 HYbrid-Coordinate Ocean Model (HYCOM). Ocean Modelling, 7(3-4): 285-322.

390 Halliwell J G R, Bleck R, Chassignet E P, 1998. Atlantic Ocean simulations performed using a
391 new Hybrid Coordinate Ocean Model (HYCOM). EOS, Fall AGU Meeting.

392 Halliwell J G R, Bleck R, Chassignet E P, Smith L T, 2000. Mixed layer model validation in
393 Atlantic Ocean simulations using the Hybrid Coordinate Ocean Model (HYCOM). EOS,

394 80, OS304.
395 Han Y–J, 1984. A numerical world ocean general circulation model: Part II. A baroclinic
396 experiment. Dynamics of Atmospheres and Oceans, 8(2):141-172.
397 Hamilton P, Fargion G S, Biggs D C, 1999. Loop Current eddy paths in the western Gulf of
398 Mexico. Journal of Physical Oceanography, 29(6): 1180-1207.
399 Jia Y, Liu Q, Liu W, 2005. Primary studies of the mechanism of eddy shedding from the
400 Kuroshio bend in Luzon Strait. Journal of Oceanography, 61(6): 1017-1027.
401 Kara A B, Rochford P A, Hurlburt H E. 2002. Air-sea flux estimates and the 1997-1998 ENSO
402 event. Boundary-Layer Meteorology, 103(3): 439-458.
403 Large W G, McWilliams J C, Doney S C, 1994. Oceanic vertical mixing: a review and a model
404 with a nonlocal boundary layer parameterization. Reviews Geophysics, 32(4): 363-403.
405 Legates D R, Willmott C J, 1990. Mean seasonal and spatial variability in gauge-corrected,
406 global precipitation. International Journal of Climatology. 10(2): 111-127.
407 Li L, Nowlin W D, Su J L, 1998. Anticyclonic rings from the Kuroshio in the South China Sea.
408 Deep-Sea Research, Part I, 45: 1469-1482.
409 Li Q Y, Sun L, 2015. Technical Note: Watershed strategy for oceanic mesoscale eddy splitting,
410 Ocean Science, 11(2): 269-273, doi:10.5194/os-11-269-2015.
411 Li Q Y, Sun L, Lin S-F, 2016. GEM: a dynamic tracking model for mesoscale eddies in the
412 ocean, Ocean Science, 12: 1249-1267, doi:10.5194/os-12-1249-2016.
413 Li Q Y, Sun L, Liu S-S, Xian T, Yan Y-F, 2014. A new mononuclear eddy identification method
414 with simple splitting strategies. Remote Sensing Letters, 5(1): 65-72.
415 Doi:10.1080/2150704X.2013.872814.
416 Li X C, 2009. Applying a new localization optimal interpolation assimilation module to
417 assimilate sea surface temperature and sea level anomaly into the Chinese Shelf/Coastal
418 Seas model and carry out hindcasted experiment. Graduate University of the Chinese
419 Academy of Sciences, 92pp.
420 Li X C, Zhu J, Xiao Y G, Wang R W, 2010. A Model-Based Observation Thinning Scheme for
421 the Assimilation of High-Resolution SST in the Shelf and Coastal Seas around China.
422 Journal of Atmospheric and Oceanic Technology, 27(6):1044-1058.
423 Liu Z, Yang H J, Liu Q, 2001. Regional dynamics of seasonal variability of sea surface height

in the South China Sea. Journal of Physical Oceanography, 31(1): 272-284.

Morrow R, Traon P-Y L, 2012. Recent advances in observing mesoscale ocean dynamics with satellite altimetry. Advances in Space Research, 50, 1062-1076.

Oey L T, Ezer T, Lee H C, 2005. Loop Current, rings and related circulation in the Gulf of Mexico: a review of numerical models. In: Circulation in the Gulf of Mexico: Observations and Models. American Geophysical Union, 31-56.

Oke P R, Allen J S, Miller R N, Egbert G D, Kosro P M, 2002. Assimilation of surface velocity data into a primitive equation coastal ocean model. Journal of Geophysical Research Oceans, 107(C9): 5-1-5-25.

Oke P R, Brassington G B, Griffin D A, Schiller A, 2010. Ocean data assimilation: a case for ensemble optimal interpolation. Australian Meteorological and Oceanographic Journal, 59: 67-76.

Reynolds R W, Smith T M, Liu Chunying, et al., 2007. Daily High Resolution Blended Analyses for Sea Surface Temperature. Journal of Climate, 20(22): 5473-5496.

Rio M. H., S. Mulet, and N. Picot, 2014: Beyond GOCE for the ocean circulation estimate: Synergetic use of altimetry, gravimetry, and in situ data provides new insight into geostrophic and Ekman currents. Geophysical Research Letters, 41(24): 8918-8925.

Treguier A M, Chassignet E P, Boyer A L, Pinardi N, 2017. Modeling and forecasting the "weather of the ocean" at the mesoscale. Journal of Marine Research, 75(3): 301-329.

Uppala S, Kallberg P, Simmons A J, et al., 2005. The EAR-40 re-analysis. Quarterly Journal of the Royal Meteorological Society, 131(612): 2961-3012.

Vos M D, Backeberg B, Counillon F, 2018. Using an eddy-tracking algorithm to understand the impact of assimilating altimetry data on the eddy characteristics of the Agulhas system. Ocean Dynamics, 1-21.

Wang D X, Zhou F Z, Qin Z H, 1996. Numerical simulation of the upper ocean circulation with two-layer model. Acta Oceanologica Sinica, 18(5): 30-40.

Wang D, Xu H, Lin J, et al., 2008. Anticyclonic eddies in the northeastern South China Sea during winter 2003/2004. Journal of Oceanography, 64: 925-935, doi: 910.1007/s10872-10008-10076-10873.

Wang G, Su J, Chu P C, 2003. Mesoscale eddies in the South China Sea observed with altimeter

454 data. Geophysical Research Letters, 30(21): 2121, doi: 10.1029/2003GL018532.
455 Wang Z, Li Q, Sun L, Li S, Yang Y J, Liu S-S, 2015. The most typical shape of oceanic
456 mesoscale eddies from global satellite sea level observations, Frontiers of Earth Science,
457 9 (2): 202-208. DOI 10.1007/s11707-014-0478-z.
458 Woodham R H, Alves O, Brassington G B, Robertson R, Kiss A, 2015. Evaluation of ocean
459 forecast performance for Royal Australian Navy exercise areas in the Tasman Sea, Journal
460 of Operational Oceanography, 8(2): 147-161.
461 Woodruff S D,Slutz R J, Jenne R L, Steurer P M, 1987. A comprehensive ocean-atmosphere
462 data set. Bulletin of the American Meteorological Society,68(10):1239-1250.
463 Wu C R, Chiang T L, 2007. Mesoscale eddies in the northern South China Sea. Deep-Sea
464 Research, Part II, 54(14): 1575-1588.
465 Xiao X J, Wang D X, Xu J-J, 2006. The assimilation experiment in the southwestern South
466 China Sea in summer 2000. Chinese Science Bulletin, 51(s2): 31-37.
467 Xie J P, Bertino L, Cardellach E, Semmling M, Wickert J, 2018. An OSSE evaluation of the
468 GNSS-R altimetery data for the GEROS-ISS mission as a complement to the existing
469 observational networks, Remote Sensing of Environment, 209: 152-165.
470 Xie J P, Counillon F, Zhu J, Bertino L, 2011. An eddy resolving tidal-driven model of the South
471 China Sea assimilating along-track SLA data using the EnOI. Ocean Science, 8(2): 609-
472 627.
473 Xu D Z, Li X C, Zhu J, Qi Y Q, 2011. Evaluation of an ocean data assimilation system in the
474 marginal seas around China, with a focus on the South China Sea. Chinese Journal of
475 Oceanology and Limnology, 29(2): 414-426.
476 Xu D Z, Zhu J, Qi Y Q, et al., 2012. Impact of mean dynamic topography on SLA assimilation
477 in an eddy-resolving model. Acta Oceanologica Sinica, 31(5): 11-25.
478 Yan C X, Zhu J, Zhou G Q, 2007. Impacts of XBT, TAO, altimetry and ARGO observations on
479 the tropic Pacific Ocean data assimilation. Advances in Atmospheric Sciences, 24(3): 383-
480 398.
481 Yang K, Shi P, Wang D X, et al., 2000. Numerical study about the mesoscale multi-eddy system
482 in the northern South China Sea in winter. Acta Oceanologica Sinica, 22(1): 27-34.
483 Zhu J, 2011. Overview of Regional and Coastal Systems, Chapter 17 in Operational

484 Oceanography in the 21st Century. Edited by A. Schiller and G. B. Brassington, PP. 727,
485 Springer Science, Business Media B.V.
486 Zhuang W, Du Y, Wang D X, Xie Q, 2010: Pathways of mesoscale variability in the South
487 China Sea. Chinese Journal of Oceanology and Limnology, 28(5): 1055-1067.
488

Figures:

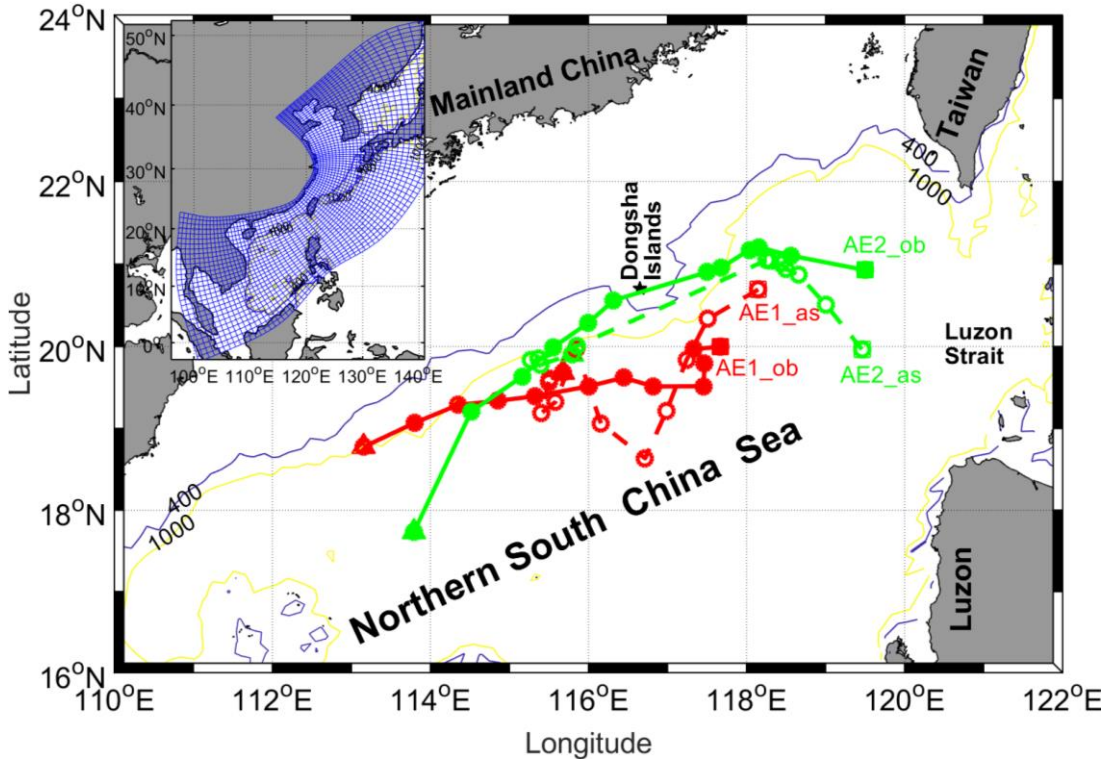

Fig. 1 Bathymetry of the northern South China Sea. The blue and yellow contour lines are the isolines of 400 m and 1000 m. The solid black Pentagram indicated Dongsha Islands. The migration path of AE1 and AE2 in the NSCS during December 2003~April 2004. Red solid (hollow) circle dots and solid (dash) lines indicated weekly passing position and migration path of observation (assimilation) AE1. Green solid (hollow) circle dots and solid (dash) lines indicated weekly passing position and migration path of observation (assimilation) AE2. The quadrangle and triangle denoted start and end position, respectively. The model domain of CSCSS (the inset panel), the curvilinear orthogonal model grid with 1/8-1/12° horizontal resolution (147×430) is denoted by the blue grid (at intervals of 10 grid cells here).

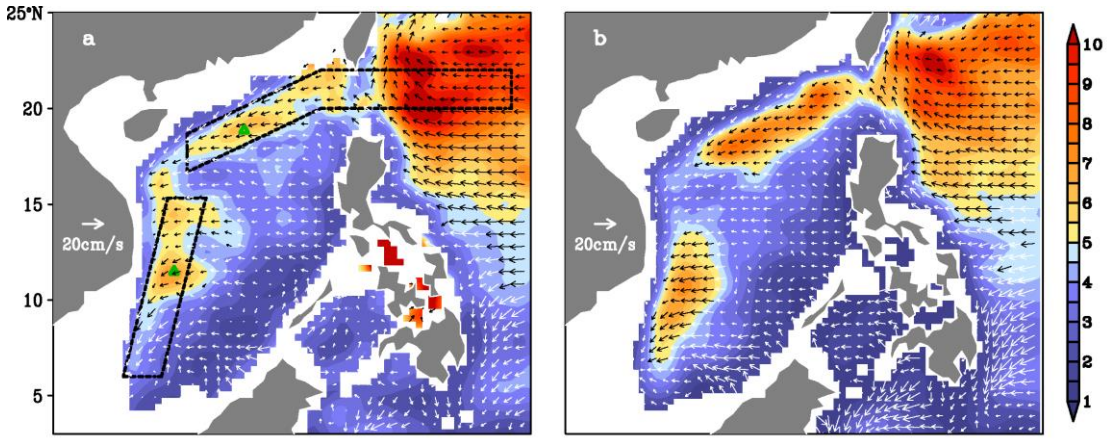

503

504 Fig. 2 Annual mean standard deviation of sea level mesoscale signals (color shading, unit: cm) and
505 propagation velocities of the signals (vectors) derived from (a) altimeter observations; (b) OFES
506 simulations. From Zhuang et al. (2010).

507

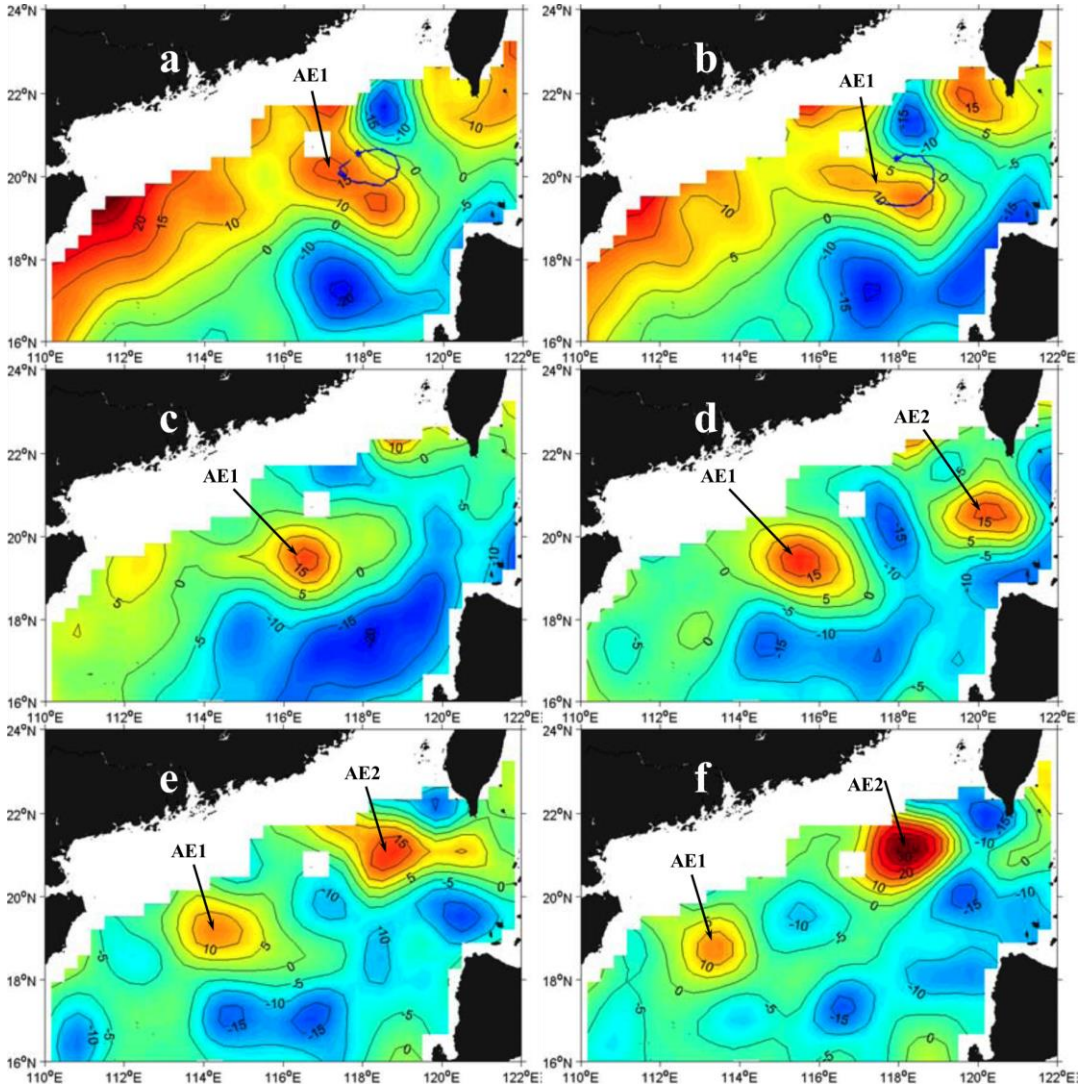

508

509 Fig. 3 Snapshots of SLA from satellite remote sensing datasets. Buoy 22918 trajectory (blue lines,
510 blue asterisk represents the initial position of buoy, as in Fig. 4) (a) from December 4–15, 2003
511 superposed on SLA field on December 10, 2003; (b) from December 16– 23, 2003 superposed on

512 SLA field on December 17, 2003; SLA field on (c) January 7, 2004; (d) January 21, 2004; (e)
513 February 4, 2004; (f) February 18, 2004. From Wang et al. (2008).

514

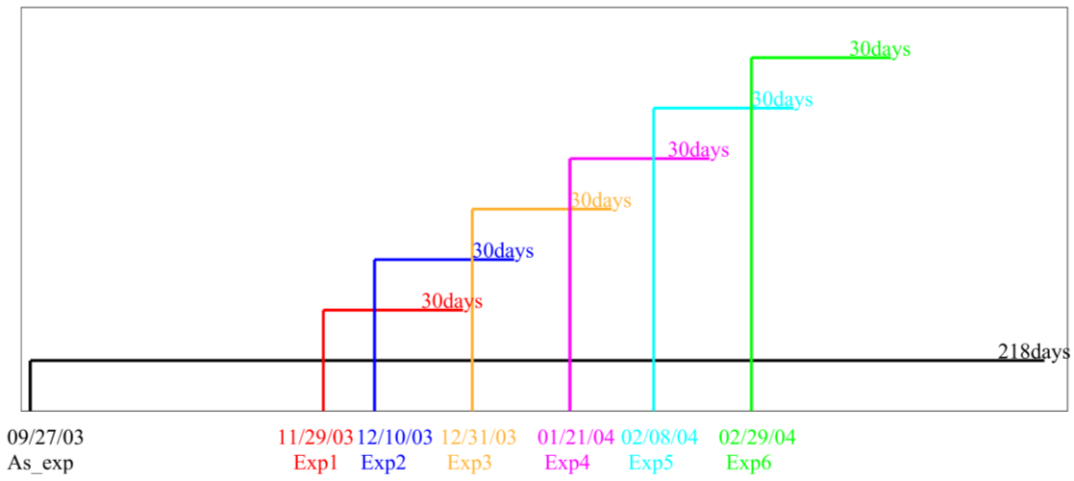

515

516 Fig. 4 The settings of assimilation and six forecast experiments, including the start and end date.

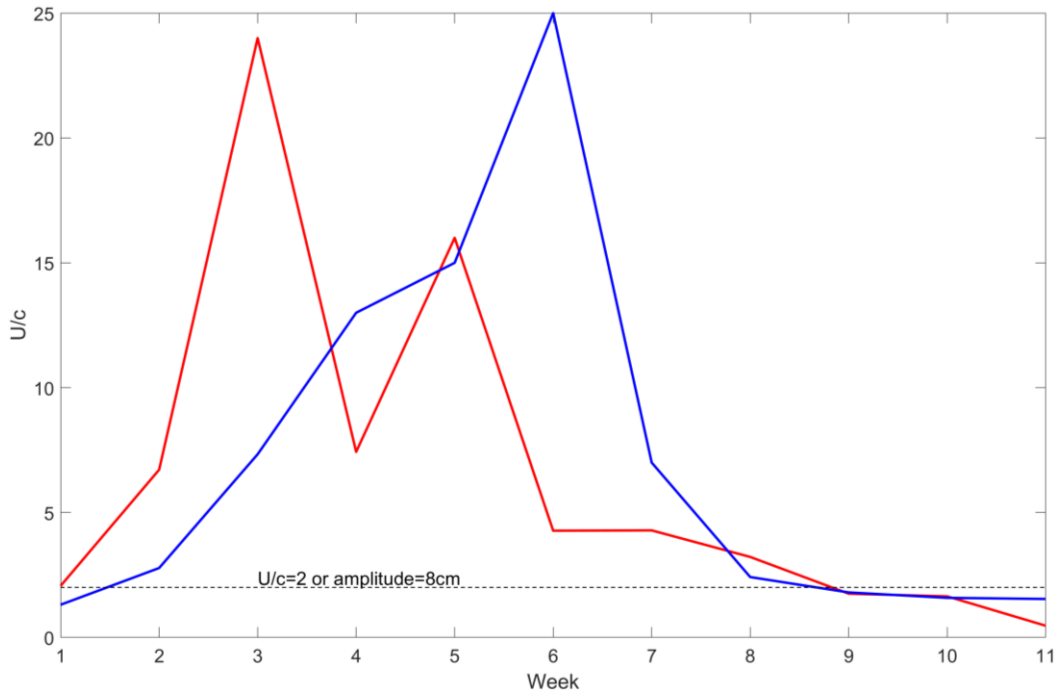

517

518 Fig. 5 The advective nonlinearity parameter. The thick red (blue) curve indicates the U/c of the
519 observed (As_exp experiment) of AE2, the dash line indicates the value of eddy amplitude at 8 cm
520 or the U/c=2.

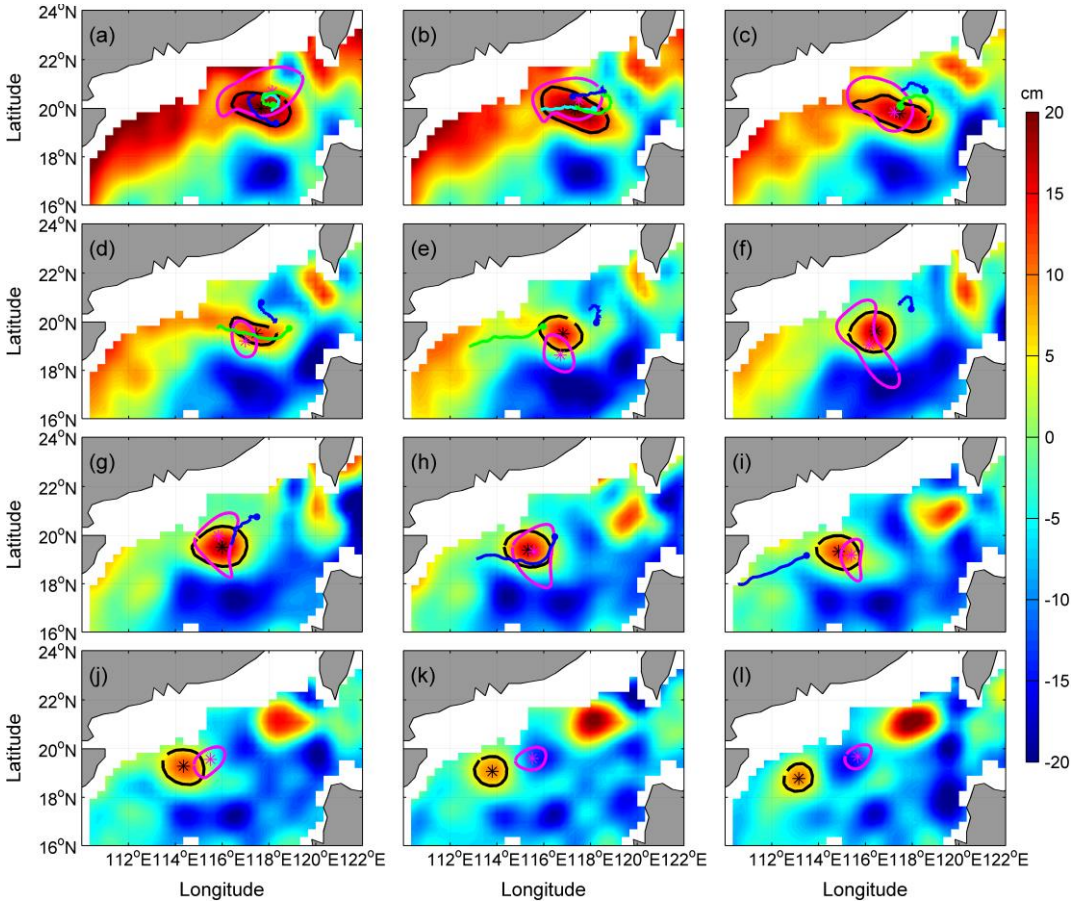

Fig. 6 Comparisons of AE1 derived from weekly SLA of assimilation results and observation from satellite remote sensing during the period of December 2003~February 2004. Background color is SLA, "*" mark and closed lines indicated the center position and the outermost closed isoline of AE1, respectively, the black is from satellite observation SLA, the pink is from assimilation SLA. The cyan, green and blue solid circle lines indicated the start positions and trajectories of number 22517, 22918 and 22610 drifter buoys, respectively. (a)-(l) is SLA on the 3rd of December 2003~ the 18th of February 2004, respectively. Unit: cm.

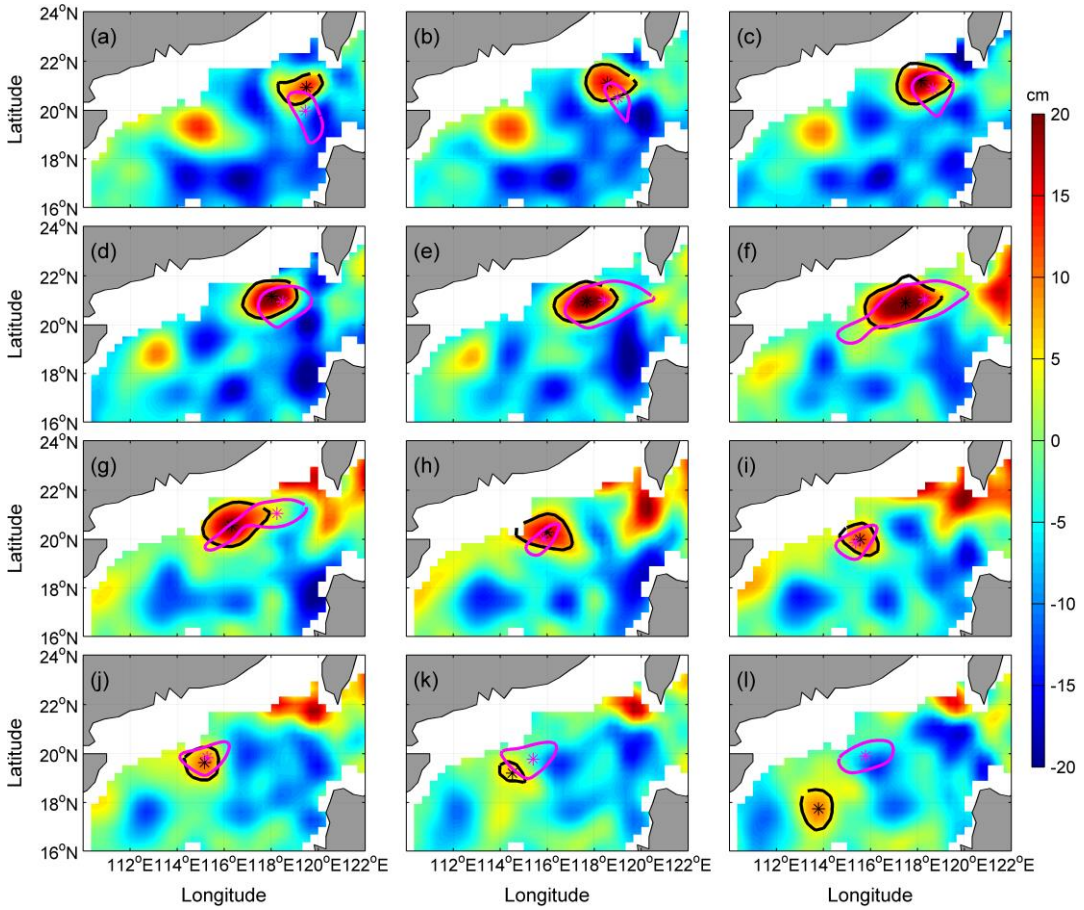

Fig. 7 The same as figure 6, But for AE2, the corresponding period is January 28th, 2003~April 14th, 2004.

Tables：

Table 1 The intensity and amplitude of AE1 and AE2 derived from observation SLA and the assimilation SLA, and distance of eddy centers between the observation SLA's and assimilation SLA's.

Weekly			1(2003/12/3)	2	3	4	5	6	7	8	9	10	11	12
AE1	Distance (km)		94	45	26	62	98	70	54	30	63	131	199	298
	Amplitude(cm)	Observed	8	10	9	8	8	13	13	11	8	8	4	6
		Assimilated	18	12	11	6	5	4	5	6	2	3	3	2
Weekly			1(2004/1/28)	2	3	4	5	6	7	8	9	10	11	12
AE2	Distance (km)		107	83	67	57	85	91	221	36	26	26	117	328
	Amplitude(cm)	Observed	7	12	18	17	17	16	15	10	7	6	N/A	6
		Assimilated	3	2	5	6	10	8	4	8	9	4	5	6

Table 2 The Amplitude of AE1 and AE2 derived from observation SLA and the six forecast SLA, and distance of eddy centers between the observation SLA's and forecast SLA's.

Weekly				1	2	3	4	5
Exp1	Distance (km)			80	58	32	68	47
	Amplitude (cm)		Observed	8	10	9	8	8
			Forecasted	14	12	14	11	12
Exp2	Distance (km)			57	22	63	51	113
	Amplitude (cm)		Observed	10	9	8	8	13
			Forecasted	12	11	6	8	10
Exp3	Distance (km)			134	85	111	130	124
	Amplitude (cm)		Observed	13	13	11	8	8
			Forecasted	2	3	3	3	N/A
Exp4	AE1	Distance (km)		32	58	111	161	231
		Amplitude (cm)	Observed	11	8	8	4	6
			Forecasted	4	2	2	2	N/A
	AE2	Distance (km)		N/A	N/A	132	95	81
		Amplitude (cm)	Observed	N/A	N/A	12	18	17
			Forecasted	N/A	N/A	N/A	6	9
Exp5	AE1	Distance (km)		188	274	287	405	503
		Amplitude (cm)	Observed	4	6	2	N/A	N/A
			Forecasted	2	2	2	2	2
	AE2	Distance (km)		69	77	102	95	226
		Amplitude (cm)	Observed	18	17	17	16	15
			Forecasted	5	7	6	6	9
Exp6	AE2	Distance (km)		91	227	277	339	453
		Amplitude (cm)	Observed	16	15	10	7	6
			Forecasted	7	9	6	4	6

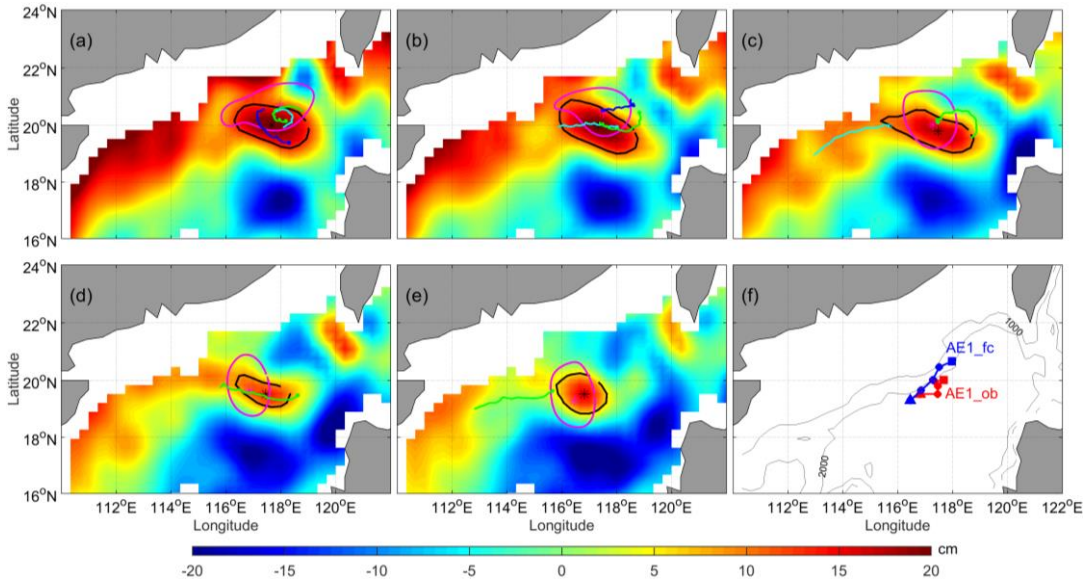

Fig. 8 Comparison of AE1 of Exp1 and observation, and trajectories of drifter buoys during the 29th of November 2003 and the 29th of December 2004. The cyan, green and blue solid circle dots and lines indicated the start positions and trajectories of number 22917, 22918 and 22610 drift buoys during the corresponding period, respectively. Where, the red (blue) dotted line in (f) is the moving path of AE1 derived from observation (forecast) SLA during the experiment period, the square (triangle) represents the start (end) position.

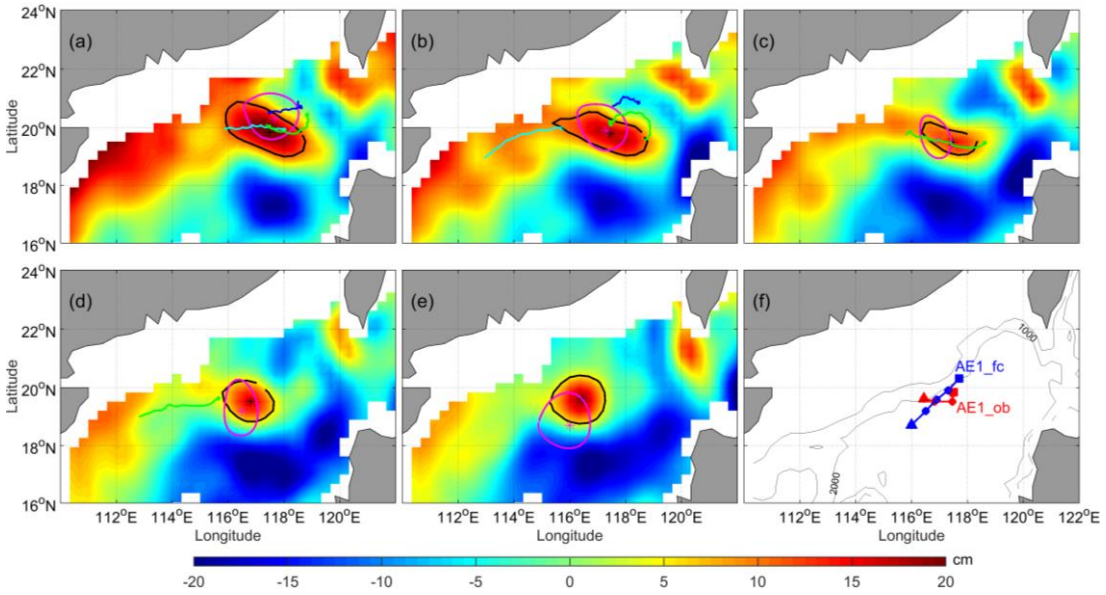

Fig. 9 Same as figure 8, but for Exp2, the experiment period is the 10th of December 2003 to the 9th of January 2004.

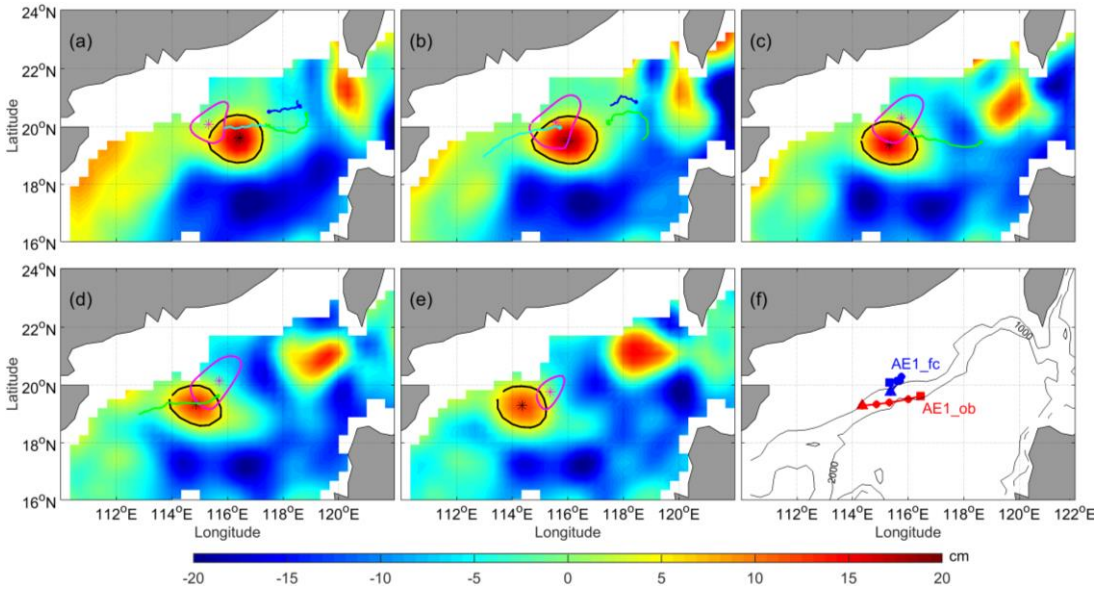

Fig. 10 Same as figure 9, but for Exp3, the experiment period is the 31st of December 2003 to the 30th of January 2004.

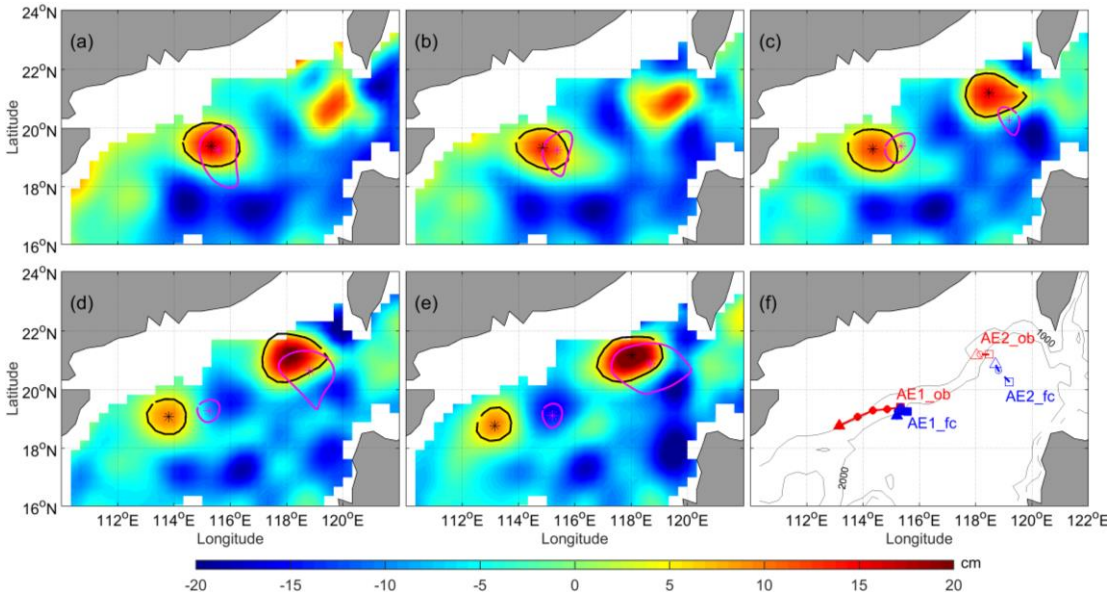

Fig. 11 Same as figure 10, but for Exp4，where, the red (blue) dotted line in (f) is the observation (forecast) moving path of AE1 and AE2. the red solid (dashed) lines and solid (hollow) circle derived from observation SLA for AE1 (AE2), the blue solid (dashed) lines and solid (hollow) circle derived from forecast SLA during the 21st of January 2004 to the 20th of February 2004.

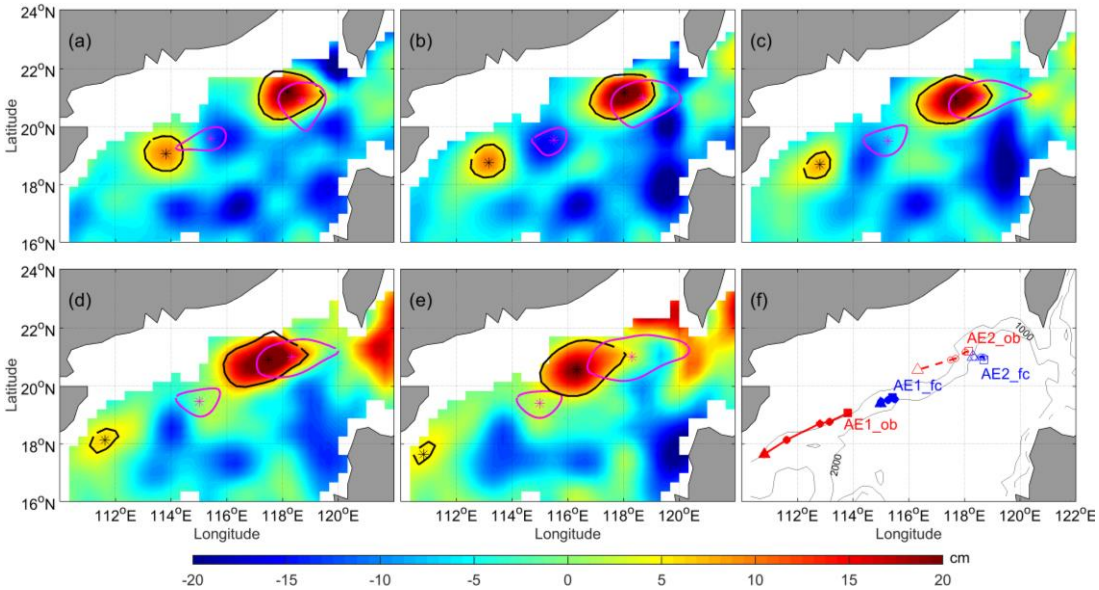

Fig. 12 Same as figure 11, but for Exp5, the experiment period is the 8th of February 2004 to the 10th of March 2004.

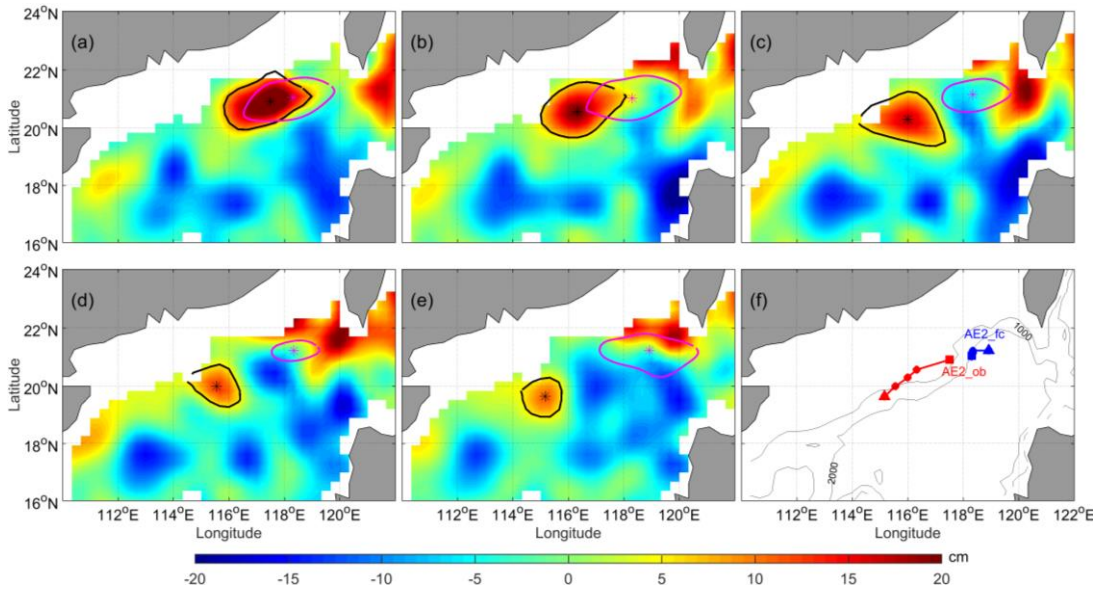

Fig. 13 Same as figure 11, but for Exp6 and AE2, the experiment period is the 29th of February 2004 to the 30th of March 2004.

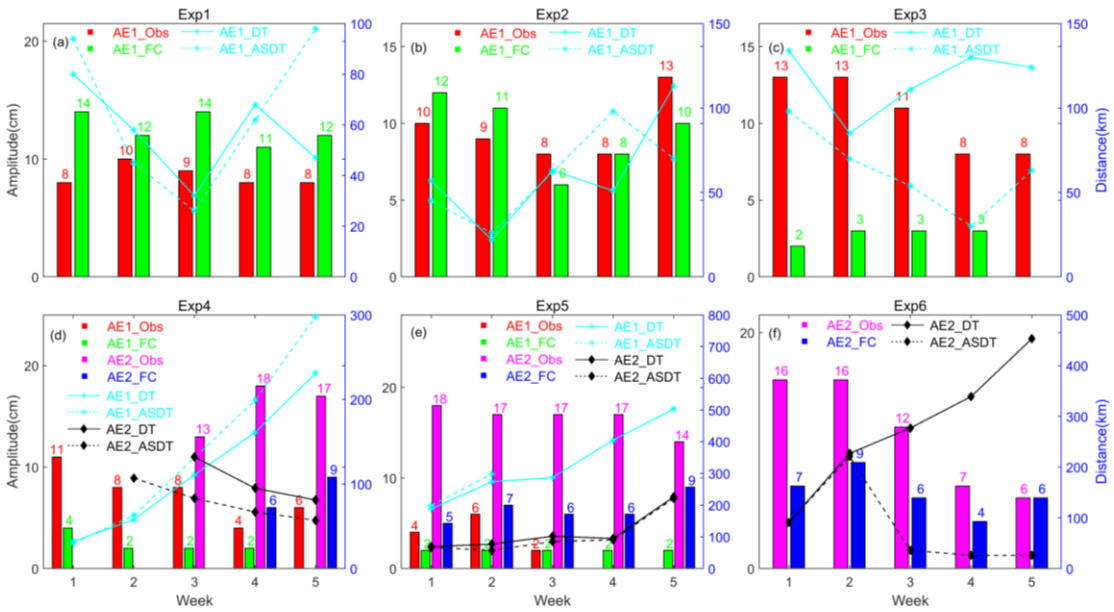

Fig. 14 The amplitude of AE1 and AE2 derived from observation SLA and the six forecast SLA, and distance of eddy centers between the observation SLA's and forecast SLA's. The red and green histograms indicated the AE1 amplitudes from observation and prediction respectively. The pink and blue histograms expressed the AE2 amplitudes from observation and prediction respectively. The cyan star solid (dash) line shows the distance of the center between observation and prediction (assimilation) AE1. The black diamond solid (dash) line shows the distance of the center between observation and prediction (assimilation) AE2.